Journal of Physics D: Applied Physics

PAPER

Low-frequency vibration suppression of a multi-layered elastic metamaterial shaft with discretized scatters

To cite this article: Lixia Li *et al* 2019 *J. Phys. D: Appl. Phys.* **52** 055105

IOP Publishing Journal of Physics D: Applied Physics
J. Phys. D: Appl. Phys. **52** (2019) 055105 (9pp) https://doi.org/10.1088/1361-6463/aaefe6

Low-frequency vibration suppression of a multi-layered elastic metamaterial shaft with discretized scatters

Lixia Li[1,2,3], Ruixiang Lv[1], Anjiang Cai[1], Miaoxia Xie[1], Yangyang Chen[2] and Guoliang Huang[2]

[1] School of Mechanical and Electrical Engineering, Xi'an University of Architecture and Technology, Xi'an 710055, People's Republic of China
[2] Department of Mechanical and Aerospace Engineering, University of Missouri, Columbia, MO 65211, United States of America

E-mail: jieli_18@163.com

Received 2 July 2018, revised 6 November 2018
Accepted for publication 9 November 2018
Published 26 November 2018

Abstract

With the aim to reduce the total structural weight, this paper presents a novel radial multi-layered elastic metamaterial (EM) shaft in which the scattering layer is circumferentially discretized into several arc-shaped sections with rotational symmetry. The dispersion relations and frequency-response-functions (FRF) of a finite structure are determined numerically first with different discretized geometries. To illustrate the mechanisms of band gaps, the eigenmodes were extracted and analyzed together with dispersion relations and FRF. The results show that in contrast to conventional multi-layered EM shafts, the proposed EM shaft with the weight being reduced by 34% can still yield broadband gaps at low-frequencies and by properly selecting the discretized geometry the band gap ranging from 139 to 197Hz exists for all three elastic wave modes. The results presented in this paper demonstrate a potential design strategy in stabilized shaft engineering.

Keywords: elastic metamaterials, local resonant, band gap, vibration control, discretized scatters

(Some figures may appear in colour only in the online journal)

1. Introduction

Phononic crystals (PCs) and locally resonant (LR) acoustic/elastic metamaterials (AMs/EMs) are types of functional structures designed to control acoustic/elastic waves in liquids/solids and have attracted growing interest due to their novel physical properties and wide range of potential applications. They have been explored for numerous engineering applications including elastic waveguides, mechanical filters, and noise isolators [1–4]. Based on the Bragg scattering mechanism [5–7], PCs have a structure period of the same order as that of the wavelength of the stop-band frequencies, such that large lattice constants are needed to reduce structural vibrations at low-frequencies, which significantly limits practical applications that do not have enough rooms [5]. To overcome this limitation, Lui *et al* proposed AMs/EMs, primarily based on the LR mechanism [8]. The three-dimensional (3D) structure consists of a heavy core with a soft epoxy matrix coating and the wavelength of the band gaps with lattice constants was found to be two orders of magnitude smaller than wavelengths at the Bragg frequency. A number of comprehensive studies on AMs/EMs can be found in the literature [9–16].

In mechanical engineering, suppressions of vibrations in rotor shafts is of great importance since strong vibrations can adversely affect the reliable operations of machines and lead to safety issues [17–21]. Various methods for reducing rotor shaft vibrations have been proposed. Earlier studies mainly focused on the design of PC materials to create a phononic

[3] Author to whom any correspondence should be addressed.

shaft [19, 20]. Richard and Pines [19] proposed a periodic shaft structure to reduce vibrations generated by the gear-mesh contact dynamics. Toso [20] suggested a stepped shaft with a periodic profile, which demonstrated effective control of vibrations at certain frequency bands. Although PC shafts are based on the Bragg mechanism, it is difficult to achieve a frequency band gap at frequencies below 1000 Hz.

In recent years, a lot of theoretical and experimental studies have been carried out on one-dimensional (1D) EM structures, such as shafts, beams, and rods with periodically attached LR oscillators, led to the discoveries and manipulations of low-frequency band gaps and thus provided a new strategy for the control of structural vibrations [22–30]. Yu *et al* [22, 23] investigated a 1D EM shaft with soft rubber rings periodically-enclosed by lead rings and determined the band gap for elastic waves. Furthermore, Wang *et al* [24–26] presented a quasi-1D EM beam with periodically attached oscillators and predicted a low-frequency band gap. However, for those conventional EM structures, low-frequency band gaps have usually been produced by using heavier LR oscillators attached to the structure, which posed a fundamental challenge in designing light-weight structures.

Various other efforts have been made to lower the band gap frequencies of 1D EM/AMs [31–36]. Huang and Sun [31] investigated band gap structures of a multi-resonator mass-in-mass lattice and showed the band gap frequency can be lowered by tuning the spring and mass of the LR oscillators. Xiao *et al* [33] introduced LR beams attached to multiple period arrays of spring-mass resonators. Meanwhile, Song *et al* [35] studied various types of periodic shafts using hard rings and LR rings, and were able to lower the flexural band frequencies. Li *et al* [36] proposed a double-layered lightweight EM shaft and showed that the weight can be reduced by 27% in contrast to the single-layered EM shaft in the same band gap range while the vibration attenuation is kept unchanged. However, in all of these studies, the LR oscillators were conservative and generally consisted of an entirely soft rubber ring covered by an entirely hard ring. Several other studies have investigated the discretization of the rubber layer in the EM structure to reduce the stiffness of the rubber coating and decrease the LR band gap frequencies [37, 38]. Cheng *et al* [37] replaced the soft rubber layer with rubber blocks in a 2D EM structure and found that the band gap frequencies could be dropped by more than one half. Moreover, Li *et al* [38] presented an EM shaft with discretized symmetric arc-shaped rubber layers, which demonstrated excellent properties for low-frequency vibrations. Although a low-frequency band gap was achieved, discretization of the rubber section resulted in less support capability and potentially cause serious eccentric problems.

This paper presents a novel radial multi-layered EM shaft in which the scattering layer is circumferentially discretized into several arc-shaped sections with rotational symmetry. The major difference between previous studies and the current manuscript is the change of the discretization on the rubber layer to the scattering layer. By making this simple change, we obtain a much more optimal design compared to previous ones, being much lighter and having similar or better vibration suppression performances. For example, compared with the single-layered EM shaft without the discretization [22], the band gap induced by the current design can be shifted to much lower frequencies, and at the same time reduce the weight of attachments by 52%. Compared with the EM shaft with discretized rubber layers [38], the shaft with discretized scattering layers have similar vibration performance, whereas the weight can be reduced by around 50%. Moreover, the discretization on the scattering layer actually introduces a new way to modify the stiffness of the rubber layer, which has not been explored before.

In this paper, a new multi-layered EM shaft is proposed with scattering layers discretized into several arc-shaped sections to further decrease the weight of the structure and, at the same time, to induce broader band gaps at much lower frequencies. Both the wave propagation behavior along infinite EM shafts and frequency-response-functions (FRF) of finite EM shafts are characterized based on numerical simulations. This paper is organized as follows: in section 2, we first introduce the design of the novel EM shaft and the numerical approach used in the following analyses; section 3 presents the numerical results of EM shafts with four and six ring layers, including band structures, eigenmodes of the EM shaft at different mode and FRFs with eight unit cells; finally, some conclusions are presented in section 4.

2. Design and modeling of the multi-layered EM shaft

The EM shaft considered in this study is comprised of a shaft with multi-layered LR ring oscillators periodically attached along the x-direction, as shown in figure 1(a). The number of layers in the radial direction is denoted as N. The cross section of the EM unit cell is illustrated in figure 1(b). The ring layers along the y-direction consists of soft rubber layers covered by hard scattering layers repeatedly. In the design, the inner hard scattering layers are discretized into several arc-sections preserving the rotational symmetry along the circumferential direction. The radius of the shaft is denoted as r_0 and the outer radius of the nth layer is denoted r_n. The arc number of every discretized arc-sections is fixed as 3. α_n represents the arc angle of discretized arc-sections in the nth layer. The material of the shaft and discretized scatters are chosen as epoxy in numerical simulations. All the material properties of the EM shaft are listed in table 1. In the calculations, the angles of the arc-scattering sections of different two scattering layers n and $n+2$ is $\theta_{n(n+2)}$. The radius of the shaft is selected as $r_0 = 0.005$ m.

Due to the geometric complexity of the presented structure, the finite element method will be applied in the calculations of dispersion relations and FRFs. The governing equations of elastic mediums can be written as

$$\sum_{j=1}^{3} \frac{\partial}{\partial x_j} \left(\sum_{l=1}^{3} \sum_{k=1}^{3} c_{ijkl} \frac{\partial u_k}{\partial x_l} \right) = \rho \frac{\partial^2 u_i}{\partial t^2} \quad (i = 1, 2, 3), \quad (1)$$

where ρ, u_i and c_{ijkl} denote the mass density, the displacement tensor and the elastic constant tensor, respectively, and

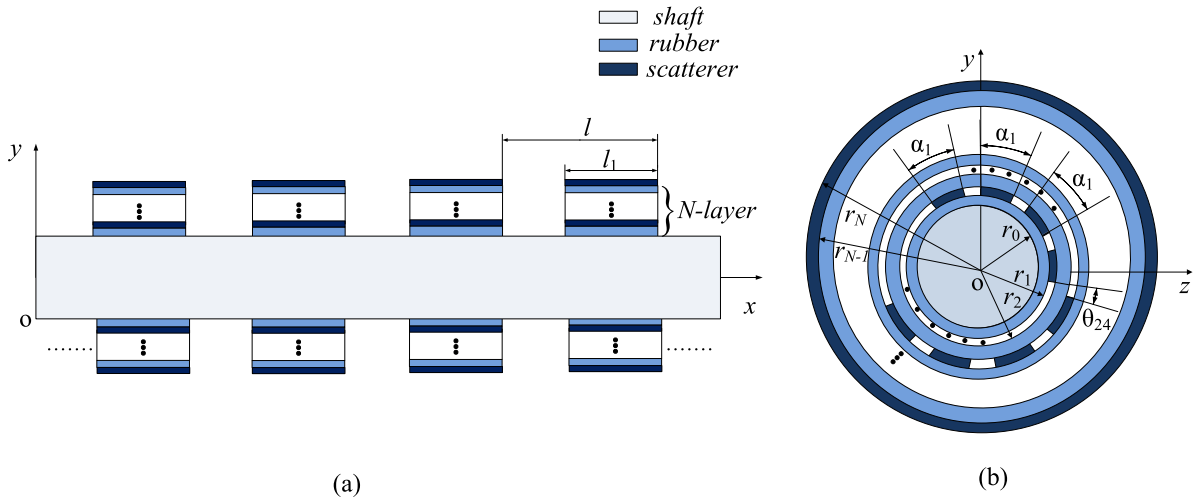

Figure 1. Schematic illustration of (a) the proposed EM shaft with LR oscillators periodically-attached and (b) the cross section of the EM unit cell.

Table 1. Material properties of the EM shaft.

Material	Density (kg m^{-3})	Shear modulus G (Pa)	Poisson's ratio λ
Epoxy	1180	1.59×10^9	0.37
Rubber	1300	3.4×10^5	0.47

x_j $(j = 1, 2, 3)$ represents the coordinate variables of x, y, and z, respectively.

The structure proposed is periodic along the x-direction and we only consider wave propagation along the x-direction such that Bloch's theorem is applied on the two boundaries of the unit cell, yielding

$$u(x + l, y, z) = u(x, y, z)\, e^{ik_x l} \tag{2}$$

where k_x is the component of the Bloch wave vector along the x-direction and l is the lattice constant. By following a standard FEM procedure, the discretized form of the eigenvalue equation for the unit cell can be written as

$$\left(K - \omega^2 M\right) u = 0 \tag{3}$$

where K and M are the stiffness and mass matrices of the unit cell, respectively, and u is the displacement at mesh nodes. By varying the value of k_x in the first Brillouin zone and solving the eigenvalue problem, the band structures as well as the eigenmode of the EM shaft can be obtained.

For the calculation of the FRF, we consider a finite structure with eight unit cells. In the simulations, forces are applied on the left boundary of the finite shaft, being normal or parallel to the surface to produce longitudinal or shear vibration modes, respectively. A torque is also applied on the left boundary to excite the rotational vibration mode. The right boundary of the finite shaft is always left free, where the corresponding displacements are measured. Finally, by varying the excitation frequency of the incident acceleration, the transmission spectra could be obtained.

3. Numerical results

3.1. The EM shaft with four ring layers

In this section, the EM shaft with four ring layers is investigated, where the inner scattering layer is discretized into three sections. The lattice constant $l = 0.075$ m, and the length of the rings $l_1 = 0.025$ m. The outer radii of the structure are selected as: $r_1 = 0.008$ m, $r_2 = 0.010$ m, $r_3 = 0.013$ m, and $r_4 = 0.015$ m, and the angle of the arc-section is $\alpha = 15°$. The band structure of the EM shaft with torsional, flexural and longitudinal wave modes in the frequency range from 0 to 1000 Hz is shown in figure 2(a). It can be clearly seen from the figure that there exists a band gap in the frequency range of 313 Hz–328 Hz for all the three modes.

To demonstrate the wave band gap mechanisms of different modes, the eigenmodes from dispersion calculations are extracted and shown in figure 3, which are labeled with letters A–G in figure 2(a), respectively. The color bar in figure 3 presents the magnitude of the total displacement field.

As shown in figure 3, for modes A and F, the host shaft experiences shear deformation supporting rotational wave modes propagated through the shaft. At low-frequencies, the attached layers, for this case, behave as a local resonator with torsional vibrations with one degree of freedom. The outer most scattering ring layer and its adjacent rubber layer acts as a lumped mass and the inner discretized scattering ring layer together with the two rubber layers work as a lumped spring with reduced stiffness compared with a whole rubber layer. As a result, an LR band gap of the torsional wave is generated at lower frequencies (152 to 523 Hz), due to the out-of-phase rotational oscillations of the outer most scattering ring layer and its adjacent rubber layer (similar to mode F). Almost the same mechanism can be found in modes B and E for longitudinal waves. Another longitudinal LR band gap is observed at low-frequencies (217 to 328 Hz), due to the out-of-phase longitudinal oscillations of the outer most scattering ring

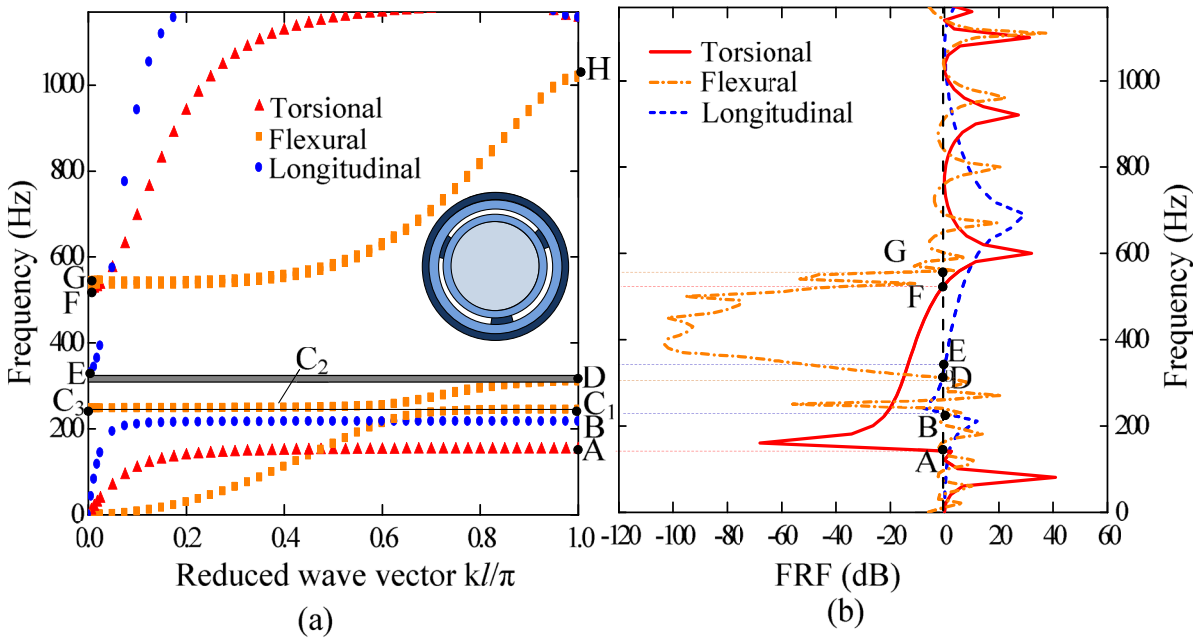

Figure 2. Illustrations of (a) the band structure and (b) the FRF of the proposed EM shaft with four ring layers where the inner scattering layer is discretized into three sections.

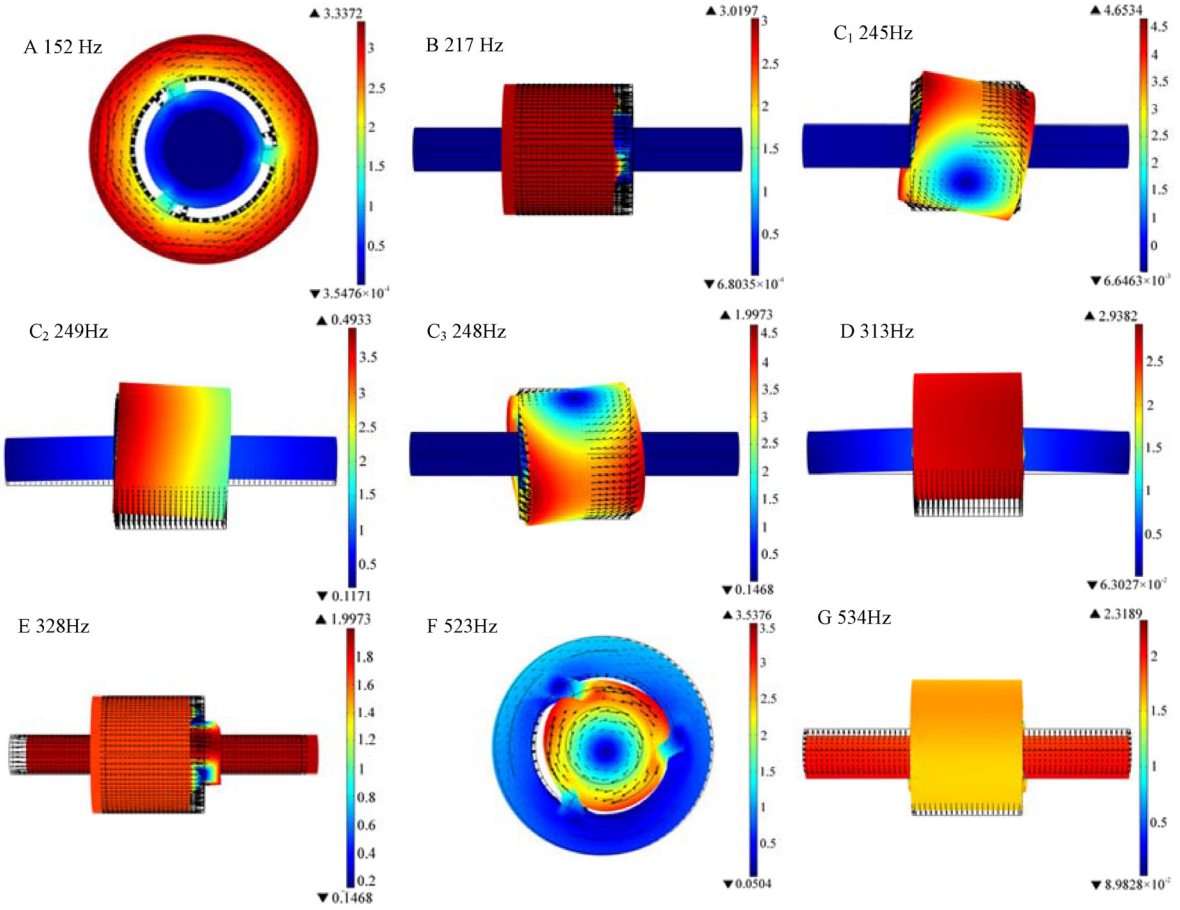

Figure 3. Images of the eigenmode shapes and displacement vector fields of the modes of figure 2(a).

layer and its adjacent rubber layer (similar to mode E). For modes D and G, the outer most scattering ring layer and its adjacent rubber layer oscillate along the *y*-direction, therefore producing a flexural wave band gap (313 to 534 Hz). Special attention should be paid on the small gap between 245–248 Hz (modes C1–C3), where the rotational oscillation of the outer most scattering ring layer and its adjacent rubber layer produces an out-of-phase bending moment to induce

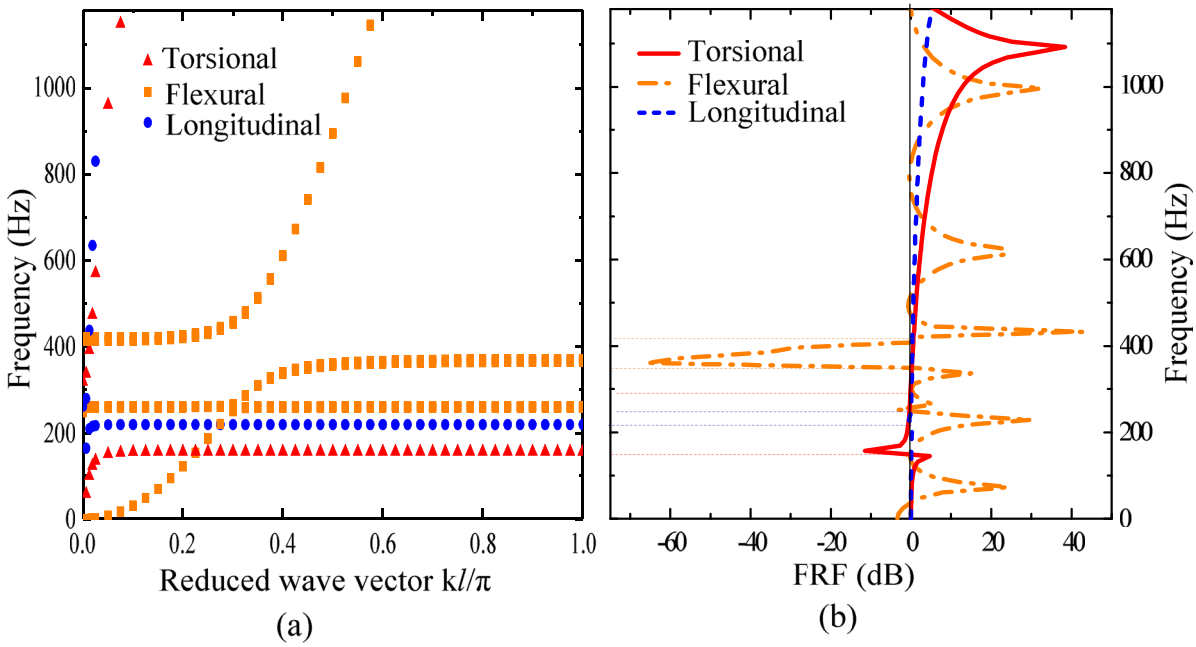

Figure 4. (a) Illustrations of (a) the band structure and (b) the FRF of a design with a steel shaft.

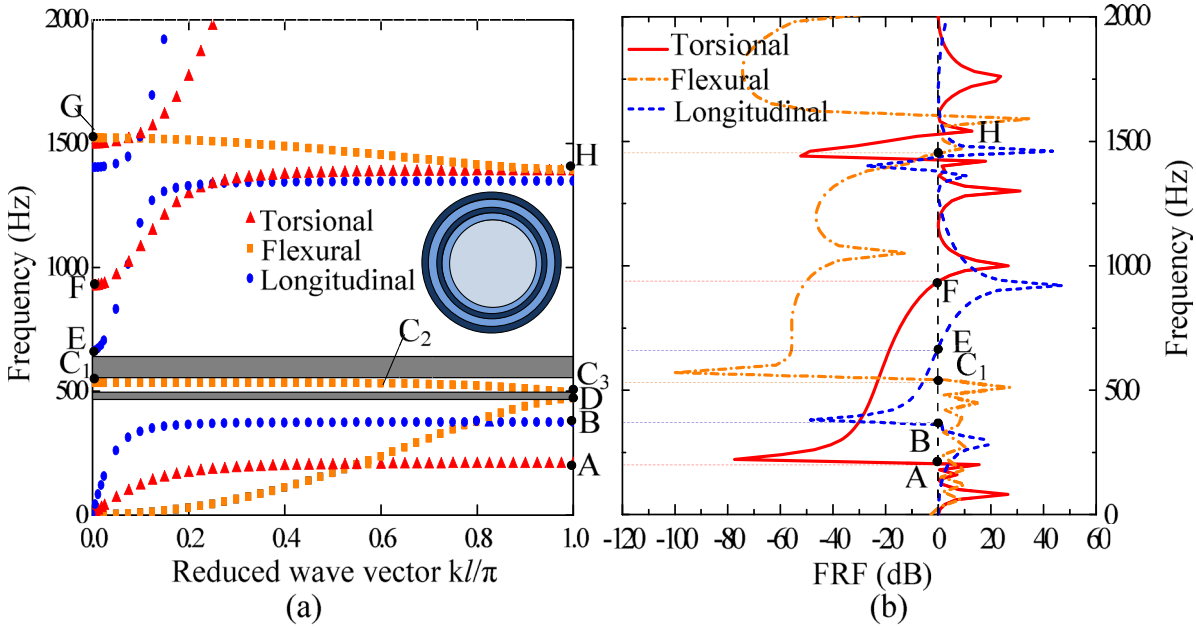

Figure 5. Illustrations of (a) the band structure and (b) the FRF of the traditional EM shaft with four ring layers.

the gap. When the frequency increases slightly (C_2), the rotational oscillation couples with translational motion. The gap therefore disappears. It should also be noted that this gap is extremely narrow, which is difficult to utilize for wave/vibration attenuations in practical designs.

To further validate the results and demonstrate the practical usage of the EM shaft, the FRF of a finite structure composed of eight unit cells is calculated in figure 2(b) with three types of harmonic loadings to generate torsional, flexural and longitudinal vibrations. As can be seen from the figure, the vibration attenuation agree very well with the band gap frequencies shown in figure 2(a) for all three modes.

Different material selections of the host shaft will not alert the working mechanism of the design. In particular, the band gap lower edge frequency will remain the same, as the local resonant frequency of the attached layers are not changed. However, the variation in the host material will modify the band gap width. To demonstrate this, figure 4 shows the dispersion relations and FRF of a design with a steel shaft, where other material parameters in the calculations are left unchanged. The density, the shear modulus and Poisson's ratio of the steel are 7780 kg m^{-3}, 8.1 $\times$ 10^{10} pa, 0.3, respectively. As expected, the band gap width becomes narrower compared to the case shown in figure 2.

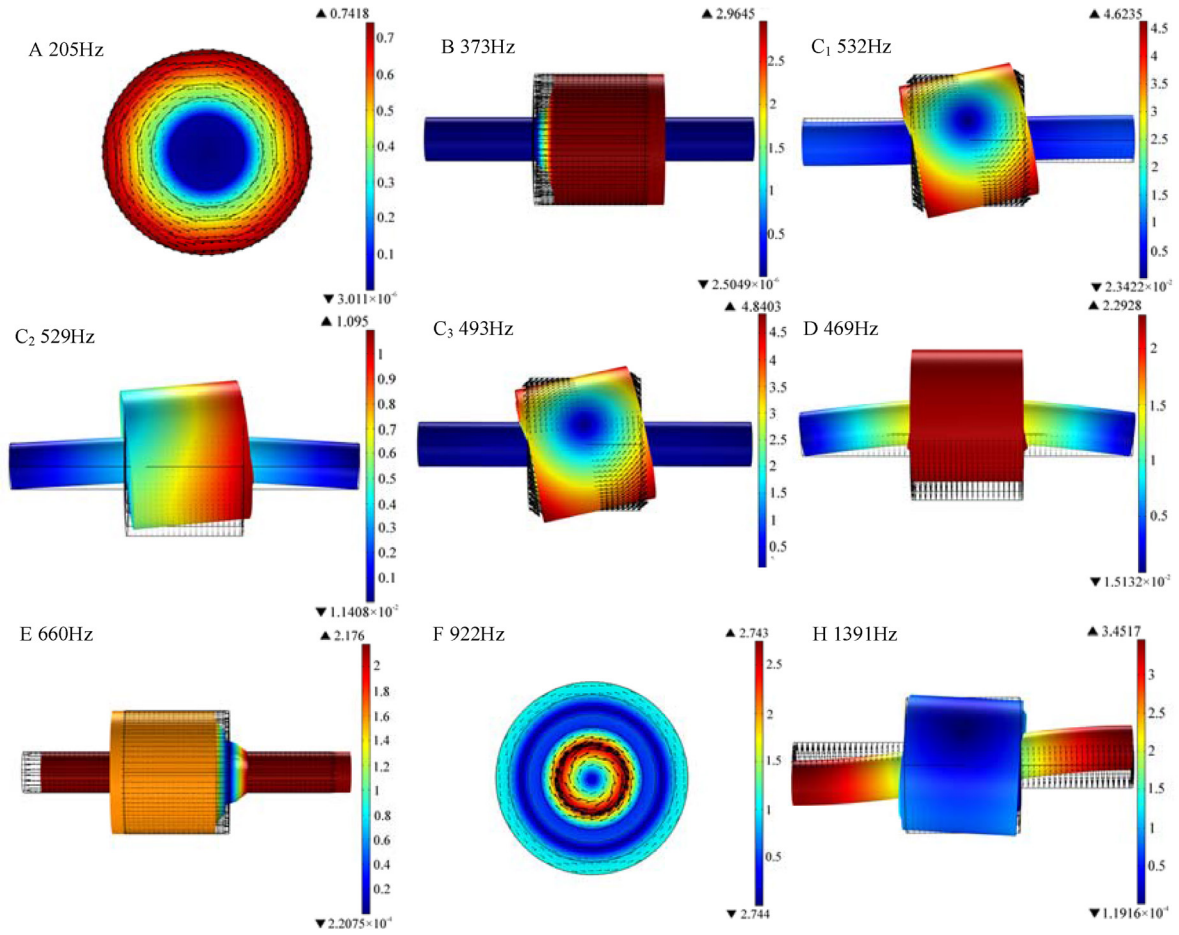

Figure 6. Images of the eigenmode shapes and displacement vector fields of the modes shown in figure 4(a).

As a comparison, the dispersion relations and FRFs of conventional EM shaft with four layers without the discretized scattering layer are studied in figure 5 and the eigenmodes from dispersion calculations are extracted and shown in figure 6. Geometric and material parameters are the same as those used in figure 2. Again, the vibration attenuation frequency regions have good agreements with the dispersion relations. Different from the proposed EM shaft, the four ring layers at the conventional EM shaft behave as local resonators with two degrees of freedom (scattering layers as lumped masses; rubber layers as lumped springs). As a result, two separate band gaps will be generated at low-frequencies for torsional and longitudinal modes, as shown in figure 5(a). For example, torsional wave band gaps are from 205–922 Hz and 1391–1496 Hz, and longitudinal wave band gaps are from 373–660 Hz and 1345–1401 Hz. However, the flexural wave band gap behavior is different from that of the torsional and longitudinal gaps. The local resonant band gap caused by the translational oscillation (mode D) is jointed together with the Bragg gap (mode H). In the frequency region from 469–1391 Hz, the structure exhibits a negative effective mass [31, 34]. It is also interested to note that a passing band appears in this band gap region. Modes C_1–C_3 demonstrate three propagating modes, where the rotational oscillations of the ring resonators are clearly observed. Those out-of-phase rotational oscillations will produce negative effective bending stiffness

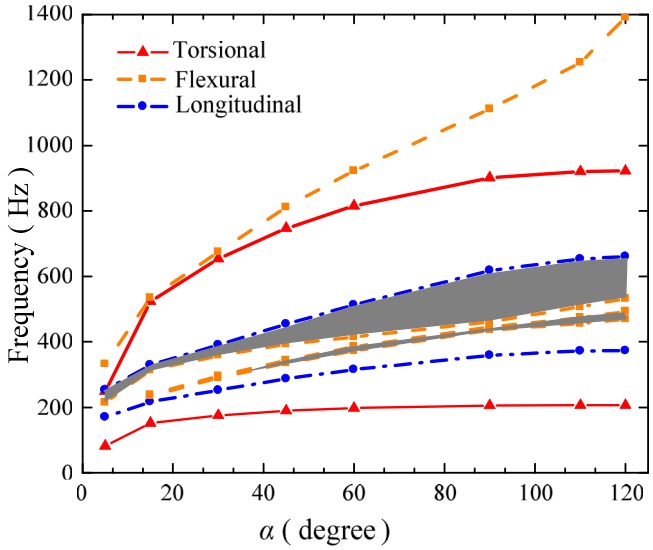

Figure 7. Graph of frequency versus arc angle showing changes in the dispersion relations due to the variation in the scattering sections introduced by the different angles.

[16] of the structure. Therefore, within this passing band, both the effective mass and effective bending stiffness are negative, where the phase velocity and group velocity are opposite as shown in figure 5(a). In addition, band gaps for all three modes can be found in the frequency ranges between 469 and

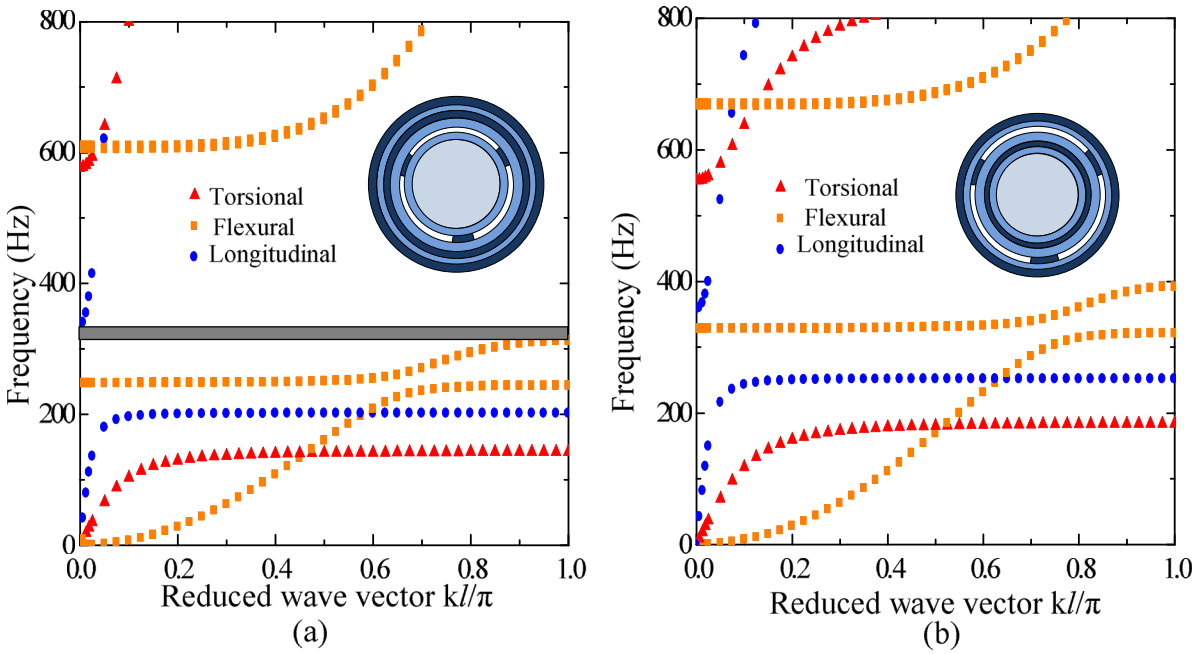

Figure 8. Illustrations of the band structure of the EM shaft with six layers where (a) only the inner-most scattering layer is discretized (b) only the middle scattering layer discretized.

493 Hz and between 532 and 660 Hz. Compared with the proposed design, the conventional EM shaft has broadband wave attenuations at higher frequencies. It should be mentioned that by introducing the discretization of the scattering ring, the proposed EM shaft not only reduces the weight of the scattering layer by 34%, but also shifts band gaps of all three modes to much lower frequencies, thanks to the decreased stiffness of the combination of the discretized scattering ring with two rubber ring layers.

With the arc number fixed at $n = 3$, the effects of the arc-section angle, α, on the band gap edge frequencies of proposed EM shaft are investigated and shown in figure 7. In the calculations, all other parameters are left unchanged. It can be seen from the figure that as the angle α decreases, the band gap edge frequencies decreases for all three modes. This is because by reducing α, the effective stiffness of the discretized scattering ring layer sandwiched between two rubber ring layers is decreased. It should be noted that when α is greater than 15°, a very narrow flexural wave band gap appears below the conventional flexural wave band gap, due to the rotational resonance. The shaded areas in the figure denote the band gap frequency regions for all three modes, in which narrower band gaps occupy lower frequency regions, and broader band gaps occupy higher frequency regions. By changing the section angle, one can manipulate the band gaps for all three modes to different frequency regions.

3.2. The EM shaft with six layers

In this section, the EM shaft with six layers is designed and investigated, where the filling ratio and the total weight of the EM shaft are the same as those of the EM shaft with four layers presented above. The geometric parameters are selected as: $r_1 = 0.005$ m, $r_2 = 0.008$ m, $r_3 = 0.010$ m, $r_4 = 0.011$ m, $r_5 = 0.013$ m, $r_6 = 0.015$ m. All the angles of the discretized arc-section all are $\alpha = 15°$.

We first investigate the case where only the inner-most scattering layer is discretized. The band structure of this EM shaft is shown in figure 8(a), in which only one complete band gap from 314–335 Hz is found. We then move our attention to the case where only the middle scattering layer discretized. The band structures of this EM shaft is again shown in figure 8(b). It can be seen from the figure that there does not exist complete band gap for this configuration. Band gaps for the torsional, flexural, and longitudinal wave are found between 184 and 553 Hz, 392 and 671 Hz, and 252 and 358 Hz, respectively, which are all slightly higher than those shown in figure 8(a), due to the increased effective stiffness in resonators with larger contact areas.

Figure 9(a) shows the band structure of the EM shaft with six layers where the inner two scattering layers are discretized with same section angles and at same positions. For the EM shaft with this geometric configuration, an arrow band gap for all the three modes is found from 290–303 Hz. In addition, the torsional, longitudinal, and flexural band gaps range from 111–340 Hz, 193–303 Hz, and 290–380 Hz, respectively. Compared with the EM shaft with four layers and the two EM structures in figure 8, all the band gaps here shift to lower frequencies while the total attached ring layers are with the same weight.

In order to obtain lower and broader band gaps for all three modes, another EM shaft with six layers is designed, where inner two scattering layers are discretized with same section angles but at different positions as the angle $\theta_{24} = 45°$ shown in figure 9(b). As the band structures also show in figure 9(b), it is interesting to notice that the lower bounds of all three band gaps are close to 100 Hz. Specifically, the band gaps for the torsional, longitudinal and flexural waves

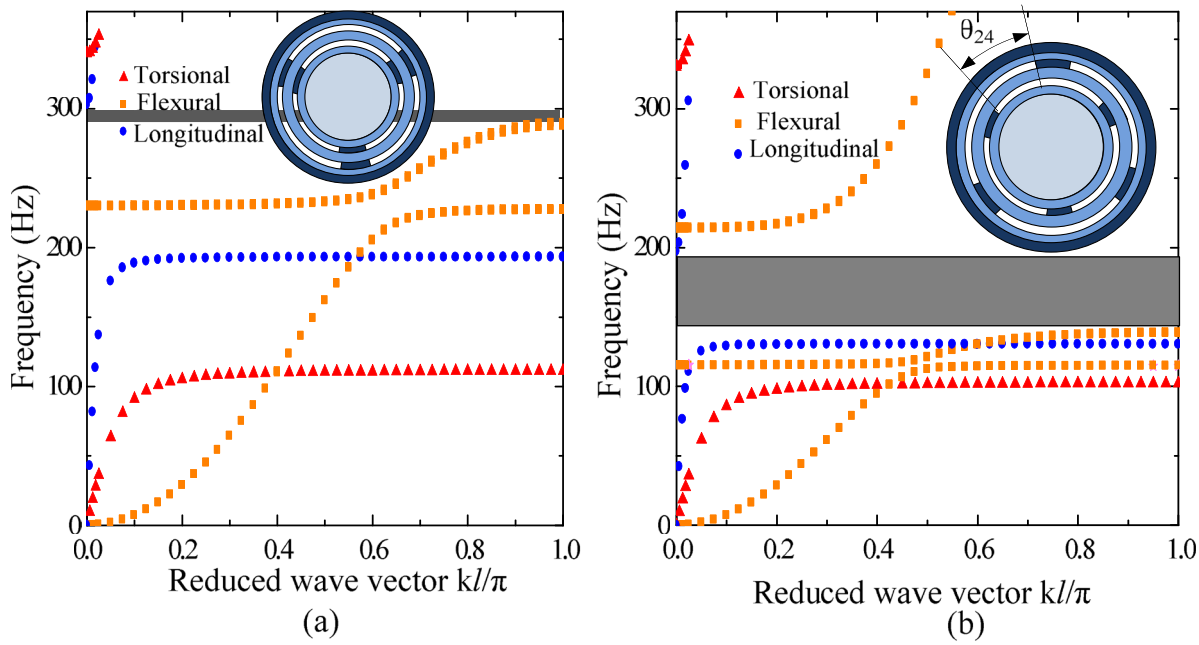

Figure 9. Illustrations of the band structure of the shaft with six layers where the inner two scattering layers are discretized at the (a) same positions, (b) different positions as the angle $\theta_{24} = 45°$.

are found between 102 and 330 Hz, 130 and 197 Hz, and 139 and 215 Hz, respectively. Furthermore, the band gap for all three modes from 139–197 Hz is much lower and broader compared with previous cases.

4. Conclusions

In this paper, we numerically investigated the band gap behavior of a novel EM shaft with discretized arc-shaped scattering layers. The dispersion relations and FRFs were calculated based on the finite element method. The eigenmodes of different elastic wave modes are plotted to interpret the band gap formation mechanism. In contrast to the conventional multi-layered EM shaft without discretization, the proposed design can produce broader band gaps at much lower frequencies but with the weight reduced by 34%. With the same filling ratio and total structural weight, increasing the number of ring layers results in increased diversity of the discretized design of the multi-layered EM shaft and better performances. Finally, the EM shaft with six layers is designed and can achieve lower and wider band gap ranging from 139–197 Hz for all three elastic wave modes. The results presented here could have potential applications in some machine design containing rotating shafts.

Acknowledgments

This work was supported by the National Natural Science Foundation of China (Grant Nos. 51405368 and 51475352) and Natural Science Foundation of Shaanxi Province (Grant No. 2017JM5024). The authors are also grateful for the support provided by the Chinese Scholarship Council (Grant No. 201607835014).

ORCID iDs

Lixia Li https://orcid.org/0000-0002-0737-3622
Guoliang Huang https://orcid.org/0000-0003-0959-8427

References

[1] Wen J, Wang G, Yu D, Zhao H and Liu Y 2005 Theoretical and experimental investigation of flexural wave propagation in straight beams with periodic structures: application to a vibration isolation structure *J. Appl. Phys.* **97** 114907
[2] Wu T, Wu L and Huang Z 2005 Frequency band-gap measurement of two-dimensional air/silicon phononic crystals using layered slanted finger interdigital transducers *J. Appl. Phys.* **97** 094916
[3] Sun J and Wu T 2007 Propagation of acoustic waves in phononic-crystal plates and waveguides using a finite-difference time-domain method *Phys. Rev.* B **76** 104304
[4] Mohammadi S, Eftekhar A, Hunt W and Adibi A 2009 High-*Q* micro-mechanical resonators in a two-dimensional phononic crystal slab *Appl. Phys. Lett.* **94** 051906
[5] Sigalas M and Economou E 1992 Elastic and acoustic wave band structure *J. Sound Vib.* **158** 377–82
[6] Kushwaha M, Halevi P, Dobrzynski L and Djafari-Rouhani B 1993 Acoustic band structure of periodic elastic composites *Phys. Rev. Lett.* **71** 2022
[7] Kushwaha M, Halevi P, Martinez G, Dobrzynski L and Djafari-Rouhani B 1994 Theory of acoustic band structure of periodic elastic composites *Phys. Rev.* B **49** 2313
[8] Liu Z, Zhang X, Mao Y, Zhu Y, Yang Z, Chan C and Sheng P 2000 Locally resonant sonic materials *Science* **289** 1734–6
[9] Goffaux C, Sánchez-Dehesa J, Yeyati A, Lambin P, Khelif A, Vasseur J and Djafari-Rouhani B 2002 Evidence of Fano-like interference phenomena in locally resonant materials *Phys. Rev. Lett.* **88** 225502
[10] Hirsekorn M and Delsanto P 2006 Elastic wave propagation in locally resonant sonic material: comparison between local interaction simulation approach and modal analysis *J. Appl. Phys.* **99** 124912

[11] Deymier P, Cardona M, Fulde P, Klitzing K, Merlin R, Queisser H and Störmer H 2013 *Acoustic Metamaterials and Phononic Crystals* (Heidelberg: Springer)
[12] Hussein M, Leamy M and Ruzzene M 2014 Dynamics of phononic materials and structures, historical origins, recent progress, and future outlook *Appl. Mech. Rev.* **66** 040802
[13] Chen Y, Huang G and Sun C 2014 Band gap control in an active elastic metamaterial with negative capacitance piezoelectric shunting *J. Vib. Acoust.* **136** 061008
[14] Chen Y and Huang G 2015 Active elastic metamaterials for subwavelength wave propagation control *Acta Mech. Sin.* **31** 349–63
[15] Ma G and Sheng P 2016 Acoustic metamaterials: from local resonances to broad horizons *Sci. Adv.* **2** 1501595
[16] Chen Y, Hu G and Huang G 2017 A hybrid elastic metamaterial with negative mass density and tunable bending stiffness *J. Mech. Phys. Solids* **105** 179–98
[17] Tan C and Kang B 1998 Wave reflection and transmission in an axially strained rotating Timoshenko shaft *J. Sound Vib.* **213** 483–510
[18] Scott R and Kim W 2001 Harmonic wave propagation in an infinite rotating composite Timoshenko shaft *J. Sound Vib.* **243** 763–8
[19] Richards D and Pines D 2003 Passive reduction of gear mesh vibration using a periodic drive shaft *J. Sound Vib.* **264** 317–42
[20] Toso M 2004 Wave propagation in rods, shell, and rotating shaft with non-uniform geometry *Doctoral Thesis* University of Maryland, College Park
[21] Hu Q, Yang C, Liu S and Zheng H 2014 Torsional vibration active control of hybrid construction machinery complex shafting *J. Cent. South Univ.* **21** 3498–503
[22] Yu D, Liu Y, Wang G, Li C and Qiu Q 2006 Low frequency torsional vibration gaps in the shaft with locally resonant structures *Phys. Lett.* A **348** 410–5
[23] Yu D, Liu Y, Wang G, Zhao H and Qiu J 2006 Flexural vibration band gaps in Timoshenko beams with locally resonant structures *J. Appl. Phys.* **100** 124901
[24] Wang G, Yu D, Wen J, Liu Y and Wen X 2004 One-dimensional phononic crystals with locally resonant structures *Phys. Lett.* A **327** 512–21
[25] Wang G, Wen J and Wen X 2005 Quasi-one-dimensional phononic crystals studied using the improved lumped-mass method: application to locally resonant beams with flexural wave band gap *Phys. Rev.* B **71** 104302
[26] Wang G, Wen X, Wen J and Liu Y 2006 Quasi-one-dimensional periodic structure with locally resonant band gap *J. Appl. Phys.* **73** 167–70
[27] Liu Y, Yu D, Li L, Zhao H, Wen J and Wen X 2007 Design guidelines for flexural wave attenuation of slender beams with local resonators *Phys. Lett.* A **362** 344–7
[28] Liu L and Hussein M 2010 Wave motion in periodic flexural beams and characterization of the transition between Bragg scattering and local resonance *J. Appl. Mech.* **79** 011003
[29] Pai P 2010 Metamaterial-based broadband elastic wave absorber *J. Intell. Mater. Syst. Struct.* **21** 517–28
[30] Xiao Y, Wen J and Wen X 2012 Longitudinal wave band gaps in metamaterial-based elastic rods containing multi-degree-of-freedom resonators *New. J. Phys.* **14** 033042
[31] Huang G and Sun C 2010 Band gaps in a multiresonator acoustic metamaterial *J. Vib. Acoust.* **132** 031003
[32] Chen Y, Hu G and Huang G 2016 An adaptive metamaterial beam with hybrid shunting circuits for extremely broadband control of flexural waves *Smart. Mater. Struct.* **25** 105036
[33] Xiao Y, Wen J and Wen X 2012 Broadband locally resonant beams containing multiple periodic arrays of attached resonators *Phys. Lett.* A **376** 1384–90
[34] Chen Y, Barnhart M, Chen J, Hu G, Sun C and Huang G 2016 Dissipative elastic metamaterials for broadband wave mitigation at subwavelength scale *Compos. Struct.* **136** 358–71
[35] Song Y, Wen J, Yu D and Wen X 2013 Analysis and enhancement of torsional vibration stopbands in a periodic shaft system *J. Phys. D: Appl. Phys.* **46** 145306
[36] Li L and Cai A 2016 Low-frequency band gap mechanism of torsional vibration of lightweight elastic metamaterial shafts *Eur. Phys. J. Appl. Phys.* **75** 10501
[37] Cheng Z, Shi Z, Mo Y and Xiang H 2013 Locally resonant periodic structures with low-frequency band gaps *J. Appl. Phys.* **114** 033532
[38] Li L and Cai A 2016 Control of the low-frequency vibrations of elastic metamaterial shafts with discretized arc-rubber layers *Japan. J. Appl. Phys.* **55** 067301